

Spin temperature concept verified by optical magnetometry of nuclear spins

M. Vladimirova,¹ S. Cronenberger,¹ D. Scalbert,¹ I. I. Ryzhov,²
V. S. Zapasskii,² G. G. Kozlov,² A. Lemaître,³ and K. V. Kavokin^{2,4}

¹*Laboratoire Charles Coulomb, UMR 5221 CNRS-Université de Montpellier, F-34095, Montpellier, France*

²*Spin Optics Laboratory, St. Petersburg State University,
1 Ul'yanovskaya, Peterhof, St. Petersburg 198504, Russia*

³*Centre de Nanosciences et de nanotechnologies - CNRS - Université
Paris-Saclay - Université Paris-Sud, Route de Nozay, 91460 Marcoussis, France*

⁴*Ioffe Physico-Technical Institute of the RAS, 194021 St.Petersburg, Russia*

We develop a method of non-perturbative optical control over adiabatic remagnetisation of the nuclear spin system and apply it to verify the spin temperature concept in GaAs microcavities. The nuclear spin system is shown to exactly follow the predictions of the spin-temperature theory, despite the quadrupole interaction that was earlier reported to disrupt nuclear spin thermalisation. These findings open a way to deep cooling of nuclear spins in semiconductor structures, with a prospect of realization of nuclear spin-ordered states for high fidelity spin-photon interfaces.

Cooling the matter down to sufficiently low temperatures has led to the discovery of various new states of matter, such as superfluidity, Bose-Einstein condensation, quantum Hall effect. Nonetheless, there is still plenty of room for new effects at the bottom of the temperature scale, where yet weaker interactions may unexpectedly show up¹. In this context, nuclear spin system (NSS) is particularly appealing. Indeed, lowest ever reached temperatures down to sub-nanoKelvin range have been demonstrated in NSS²; exotic states characterized by negative spin temperatures have been realized, and magnetic ordering was shown to depend on the sign of the spin temperature, resulting in a rich spin phase diagram^{3,4}, due to lower (as compared to electrons) temperature of magnetic ordering, the NSS is considered as the best candidate for below-1 mK thermometry⁵⁻⁷.

Thermodynamic framework has been successfully employed for the description of a variety of the experimental data, but it becomes vital only at low magnetic fields B , of order of or less than B_L , the local field induced by the fluctuating nuclear spins. In this regime, the system can not be described in terms of statistical ensemble of individual spins, but must be treated as an element of the statistical ensemble representative of its properties⁸. To check rigorously the validity of the spin temperature hypothesis as applied to a specific system, measuring the polarization P_N of the NSS as a function of slowly varying across zero magnetic field B is required. Indeed, the behaviour of P_N during adiabatic transformation is uniquely determined by the spin temperature Θ_N , as directly follows from the second law of thermodynamics. However, most of measurements in metals^{4,7}, insulators⁹⁻¹¹ and semiconductors^{12,13} were realized at a sufficiently strong magnetic field $B \gg B_L$ where spin temperature concept becomes either trivial^{8,14}, or not applicable^{15,16}. In bulk semiconductors, the measurements of nuclear spin temperature via polarization degree of photoluminescence (PL) are scarce and made only at fixed values of the magnetic field $B \sim B_L$ ¹⁷. The only experiments where magnetisation of the NSS was

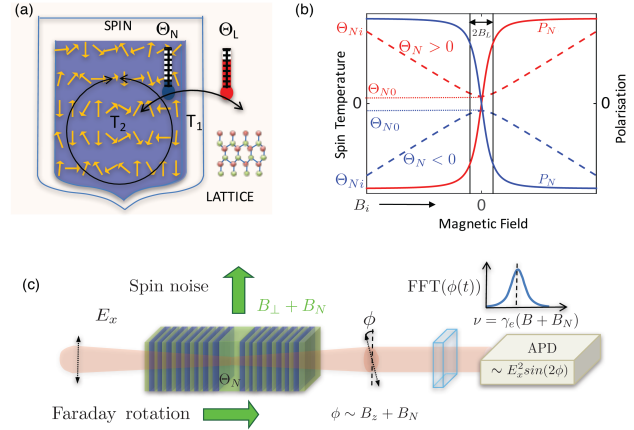


FIG. 1. (a) Sketch of the two heat reservoirs, the atomic lattice at temperature Θ_L , and the NSS at temperature Θ_N . (b) Evolution of the nuclear spin temperature (dashed lines) and polarisation (solid lines) in the adiabatic de(re)-magnetisation process starting from either positive (red lines) or negative initial spin temperature. (c) Schematic view of the sample and the detection stage of FR and SN experiments. SN spectrum is obtained as Fourier transformation of the stochastic Faraday rotation. The spectral peak frequency is directly related to the Overhauser field acting on electrons in the presence of the in-plane magnetic field.

directly measured during adiabatic scan of the magnetic field across zero showed that in semiconductor quantum dots nuclear spin temperature failed to establish due to strong quadrupole-induced local fields¹⁸.

In this Letter, we report on realization of such a proof-of-concept experiment in microcavities, semiconductor microstructures with enhanced light-matter coupling¹⁹. To this end, we develop two complementary methods of non-perturbative optical control over adiabatic transformation of the NSS, based on the Faraday rotation. Our results show that strain-induced nuclear quadrupole splittings in semiconductor microcavity do not hinder the

establishment of the thermodynamic equilibrium within the NSS. These findings open a way to deep cooling of nuclear spins in semiconductor structures, with a prospect for nuclear spin ordering^{10,11,20} and in particular, semiconductor-specific collective nuclear-spin states such as the nuclear magnetic polaron^{21,22}, or other unforeseen collective phenomena. Such states may be of interest for potential applications where spin fluctuations must be harnessed, such as high fidelity spin-photon interfaces^{23–26}, or spin-based information storage and processing.

The hypothesis of nuclear spin temperature is illustrated in Fig. 1(a,b). It states, that in a system of interacting nuclear spins isolated from the lattice an equilibrium state characterized by the temperature Θ_N will be established within a characteristic time $T_2 \approx h/\gamma_N B_L$, where γ_N is the nuclear gyromagnetic ratio. On time scales larger than T_2 and shorter than T_1 , and provided that $T_2 \ll T_1$, where T_1 is spin-lattice relaxation time, the NSS can be considered as isolated from the lattice. Θ_N can be made different from the lattice temperature $\Theta_N \neq \Theta_L$ e. g. by optical pumping^{17,27}. Depending on the mutual orientation of the pump helicity and magnetic field, NSS can be prepared either at negative or positive temperatures (nuclear spins are polarized parallel or antiparallel to B).

If NSS is prepared at temperature Θ_{N_i} under magnetic field B_i/ggB_L and subjected to a slowly varying magnetic field, such that $dB/dt < B_L/T_2$, then Θ_N and the nuclear spin polarisation P_N change obeying universal expressions^{8,17,28}:

$$\Theta_N / \sqrt{B^2 + B_L^2} = \Theta_{N_i} / B_i; \quad P_N = \frac{B}{3k_B \Theta_N} \hbar \langle \gamma_N (I+1) \rangle \quad (1)$$

based only on the principle of entropy conservation in a thermodynamic system during adiabatic process. Here I is the nuclear spin, angular brackets denote the averaging over all nuclear species, k_B is the Boltzman constant.

One can see in Fig. 1(b), that during adiabatic demagnetization of the NSS down to $B \approx B_L$ its polarization (either positive or negative, depending on the sign of Θ_{N_i}) remains constant, while the absolute value of the spin temperature decreases. This constitutes the basis for the nuclear spin cooling by adiabatic demagnetisation, a widely used cryogenic technique^{4–7}. Below B_L , nuclear polarization goes linearly to zero, the slope being directly related to $\Theta_{N_0} = \Theta_{N_i} B_L / B_i$, the spin temperature reached at $B = 0$. Subsequent application of the magnetic field in the opposite direction results in the build-up of P_N also with the opposite sign, and its absolute values are fully restored at $B \gg B_L$ ²⁹. We present below the measurements of P_N in n-doped GaAs microcavities during such adiabatic remagnetization process and compare the results to Eqs. (1).

The principle of our experiment is sketched in Fig. 1(c). Prior to the measurement, the NSS of the n-GaAs layer embedded in a microcavity (quality factor $Q \sim 20000$) is polarized by optical pumping in the

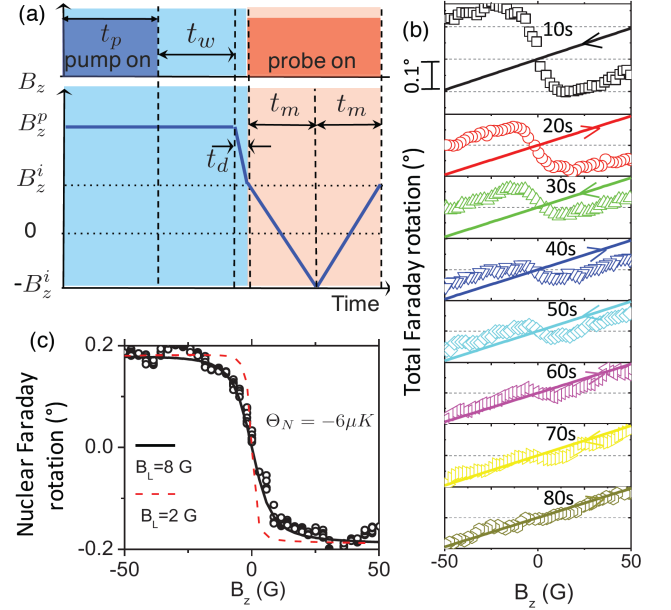


FIG. 2. Nuclear spin magnetometry by FR. (a) Timeline of the experiment: preparation (blue area) by pumping under longitudinal magnetic field B_z^p , waiting for eventual nuclear relaxation in the vicinity of the localized electrons during t_w and fast demagnetization down to B_z^i ; Faraday rotation of the probe beam is measured during successive scans of the magnetic field across zero (pink area, only first scan is shown). (b) Raw measurements of the FR in Sample B (symbols). During eight successive scans of the magnetic field (total duration 80 s, $2t_m = 10$ s, direction shown by arrows) conventional FR remains constant (contribution shown by solid lines). The remaining contribution to the signal is due to the nuclear spin polarisation. It is shown separately in (c) for the first scan (circles). Solid line is calculated from Eqs. (1).

presence of the longitudinal magnetic field. Then P_N is probed by a linearly polarized light beam tuned to the cavity mode, engineered in the transparency band of GaAs. Polarization of the light beam transmitted through the cavity is sensitive to the *Overhauser field* B_N , an effective magnetic field created by NSS and acting on electron spins³⁰. Two methods of nuclear polarization detection are used, both based on the Faraday effect, that is a rotation of the light polarization plane upon reflection (transmission) from the magnetised media: (i) the Faraday rotation induced by the Overhauser field^{31–33} and (ii) the spin noise spectroscopy of resident electrons subject to the Overhauser field^{34–37}. Details on the experimental techniques and the samples are given in Supplemental Material (SM).

The main features of the behavior of the optically cooled NSS under varying external magnetic fields are demonstrated in the experiment where the Faraday rotation angle is measured while ramping the longitudinal magnetic field across zero (Fig. 2). The experiment is conducted in two steps: preparation, including optical

pumping of nuclei at $B_z^p = 180$ G during $t_p = 15$ min, waiting for eventual nuclear relaxation in the vicinity of the localized electrons during $t_w = 1$ min, initial fast demagnetisation to $B_z^i = 50$ G during $t_d < 1$ s, and measurement under magnetic field B_z varying between B_z^i and $-B_z^i$ ³⁸.

The signal detected during eight consecutive scans of B_z is shown in Fig. 2(b). The duration of each scan is 10 s. Two distinct contributions into this signal can be identified: Faraday rotation directly induced by the external field (shown by solid lines, it remains unchanged for all the scans), and the FR ϕ_N induced by the Overhauser field, $\phi_N \propto P_N$. It is shown separately in Fig. 2(c) for the first scan. In each consecutive scan, ϕ_N diminishes due to the nuclear spin-lattice relaxation (which can be easily taken into account in the model³⁹), but the behavior of nuclear polarization is perfectly described by Eqs. (1): the polarization is an odd function of the applied field, there is no remanent magnetisation at $B = 0$, and $B_L = 8 \pm 2$ G (solid line in Fig. 2(c)). We have performed such analysis for two samples with different concentrations of Si donors n_d : an insulating sample with $n_d = 2 \cdot 10^{15} \text{ cm}^{-3}$ (Sample A) and a sample characterized by a metallic conductivity ($n_d = 2 \cdot 10^{16} \text{ cm}^{-3}$, Sample B), for NSS prepared either at positive, or at negative spin temperature (see SM). The value of B_L obtained for both samples is the same within our experimental accuracy, but far above the value expected for the local field due to dipole-dipole interactions $B_{dd} = 1.5 \text{ G}$ ⁴⁰.

We complemented these results by spin-noise measurements of nuclear remagnetisation under magnetic field perpendicular to the light and the structure axis (Fig. 3). In these experiments, the pumping stage is almost identical to the Faraday rotation experiment described above, except for the presence of a small transverse component of the magnetic field B_\perp^i . For the measurements of the SN spectra, B_z is reduced to zero, and the transverse component of the field B_\perp is tuned across zero from -50 to 50 G.

Color maps in Fig. 3(a,b) show the evolution of the electron spin noise spectra under varying magnetic fields in Sample A⁴¹. Each spectrum at a given B_\perp is characterized by a narrow peak at the frequency $\nu = \gamma_e(B_\perp + B_N) = \gamma_e(B_\perp + b_N P_N)$ of the electron Larmor precession in the total effective magnetic field acting upon the electron spins³⁴. Here $\gamma_e = 0.64 \text{ MHz/G}$ is the gyromagnetic ratio of the electrons in the conduction band of GaAs, and $b_N = 5.3 \text{ T}$ is the Overhauser field at saturation of NSS magnetization in GaAs.³⁰ Therefore the peak frequency in Fig. 3 contains two contributions: conventional SN frequency in the presence of the applied magnetic field and that induced by P_N . Depending on the sign of P_N (or, equivalently Θ_N), the resulting SN peak frequency is given either by the sum ($\Theta_N > 0$, Fig. 3 (a)) or by the difference ($\Theta_N < 0$, Fig. 3 (b)) of these two contributions. The asymmetry of the recorded sets of spectra with respect to zero magnetic field is due to nuclear spin-lattice relaxation. It has been taken into

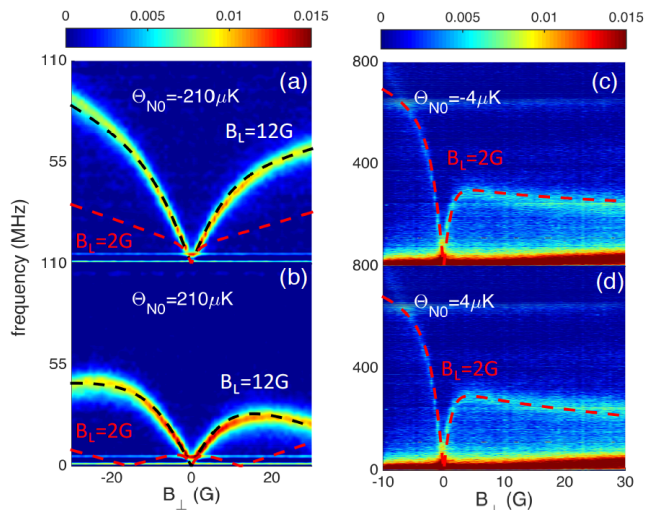


FIG. 3. Color maps of the SN spectra (in the signal to shot noise ratio units) during adiabatic demagnetisation procedure at positive (a, c) and negative (b, d) spin temperature for the microcavity sample A (a, b) and bulk sample C (c, d). Black lines in (a, b) and red line in (c, d) are fits to Eqs. 1, that determine the values of B_L and Θ_{N0} indicated on the figure (see also SM). Red lines in (a, b) illustrate how the value $B_L = 2$ G fails to describe the experiment.

account when fitting the model to the data³⁹. We obtain for both samples and both signs of the nuclear spin temperature, the value of the local field $B_L = 12 \pm 2 \text{ G}$.⁴²

Thus, the NSS does obey the prediction of the thermodynamic theory expressed by Eqs. (1), but value of the local field is surprisingly large, $B_L \gg B_{dd}$. To illustrate the difference between the observed strength of the local field B_L and B_{dd} we added in Fig. 3(a,b) the behavior of the electron SN frequency expected in the case of $B_L \approx B_{dd}$ (red line).

To elucidate the origin of this striking discrepancy, we performed SN measurements with the bulk GaAs layer without a microcavity⁴³, Sample C (Fig. 3(c,d)). Although the signal is much weaker, and the spectral line is much broader, presumably due to the inhomogeneity of the nuclear field across $20 \mu\text{m}$ -thick layer, the field dependence of the spin noise resonance is well resolved. The best fit using Eqs. (1) and with allowance for spin-lattice relaxation during the measurement³⁹ yields $B_L = 2 \text{ G}$ and $\Theta_{N0} = \pm 4 \mu\text{K}$. The record cooling down to $\Theta_{N0} = 2 \mu\text{K}$, slightly below the values reported in Ref.¹⁷, was achieved in Sample C⁴⁴.

The above comparison shows unambiguously the enhanced value of local field in the microcavities, compared to that in the bulk GaAs. Within the thermodynamic description of the NSS, the local field that enters Eqs. (1) is defined as¹⁴:

$$B_L^2 = \text{Tr}(H_S^2) / \text{Tr}(M_S^2), \quad (2)$$

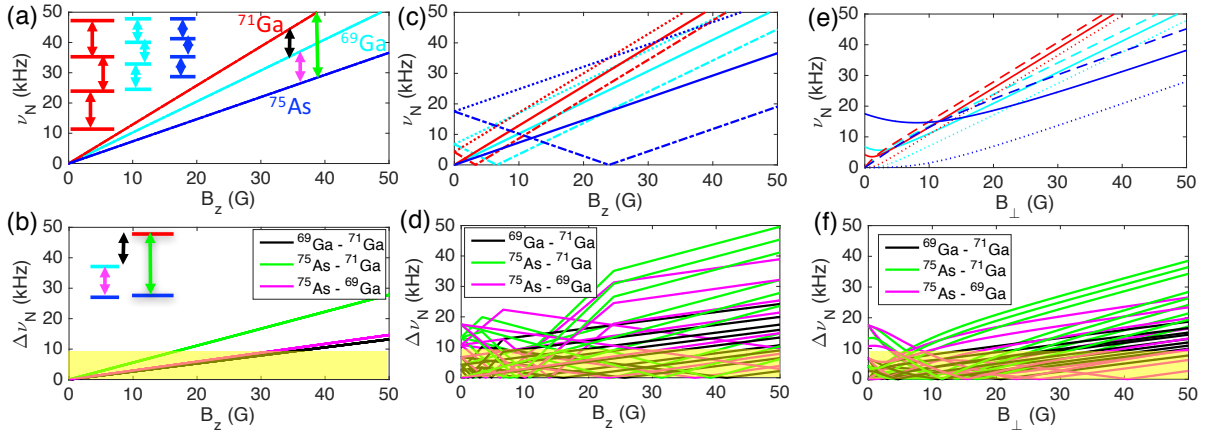


FIG. 4. (a) Nuclear spin flip transition frequencies ν_N for three GaAs isotopes, and (b) the differences $\Delta\nu_N$ between them as functions of magnetic field in the absence of the quadrupole splitting. (c-f) Same as (a) and (b), but in the presence of the quadrupole splitting in the growth direction. Magnetic field is applied either parallel (c, d) or perpendicular (e, f) to the quadrupole splitting axis. The yellow areas $\Delta\nu_N < 8$ KHz in (b, d, f) indicate the range of $\Delta\nu_N$, where inter-isotope transitions are possible.

where H_S is the Hamiltonian of all nuclear spin interactions, excluding Zeeman part (typically it includes the magnetic dipole-dipole interactions and the indirect exchange), and M_B is the parallel to the magnetic field component of the nuclear magnetic moment. In n-GaAs, magnetic dipole-dipole interaction is well-studied, and $B_L = 2$ G measured in bulk GaAs agrees well with the previous estimations for B_{dd} ⁴⁰.

The only plausible explanation for the unexpectedly strong local field detected in microcavities is the quadrupole splitting $h\nu_Q$ of the nuclear spin states induced by an uniaxial strain. In Eq.(2) it can be accounted for by introducing $H_S = H_{dd} + H_Q$, where H_Q is the Hamiltonian of the quadrupole interaction

$$H_Q = \sum_{i=1}^3 \frac{h\nu_Q^i}{2} (\hat{I}_z^2 - \frac{I(I+1)}{3}). \quad (3)$$

Here the index i stands for the summation over the three isotopes (^{69}Ga , ^{71}Ga , ^{75}As), and \hat{I}_z is the projection on the nuclear spin operator on the growth (strain) axis. Using Eq. (2) and the parameters of strain-induced quadrupole splittings in GaAs⁴⁵, one can estimate that the strain as weak as 0.01% induces the local field $B_L = 10$ G in GaAs⁴⁶.

Because this quadrupole-induced local field $B_L \gg B_{dd}$, it is the quadrupole interaction that determines the capacity of the NSS to store the energy in the internal degrees of freedom. This means that the heat capacity C_N of the NSS is 50 times larger in the microcavity samples than in bulk GaAs, because $C_N \propto B_L^2$ ¹⁴. But in contrast with dipole-dipole interaction, the quadrupole interaction does not provide any coupling between the spins, and cannot establish the thermodynamic equilibrium within the NSS. Indeed, in quantum dots,

where strong quadrupole-induced local fields have been reported, nuclear spin temperature failed to establish¹⁸. The main manifestations of this effect were the remanent magnetization at zero magnetic field, and the irreversibility of the magnetization in the course of consecutive scans of the magnetic field across zero. This is in striking contrast with our results, that show neither any loss of magnetisation, nor remanent magnetisation in zero magnetic field. From our data we can infer that Zeeman (for each of three isotopes) and internal energy reservoirs come to equilibrium between each other at fields higher than the studied range of ± 50 G. This is quantified by the value of the mixing field $B_m > 50$ G (see SM)⁴. The observed adiabaticity of the nuclear remagnetization may have either thermodynamic or quantum mechanical (Ehrenfest) interpretation⁸. However, in the Faraday configuration Zeeman and quadrupole Hamiltonians commute, which makes quantum-mechanical energy conversion impossible. The energy transfer between Zeeman and quadrupole reservoirs can only go via stochastic dipole-dipole interactions. For this reason, our experiments must be interpreted within the thermodynamic framework, with quadrupole interaction providing energy storage, and dipole-dipole interaction responsible for thermalization within the NSS.

The question remains, how can the thermodynamic equilibrium be established under magnetic field much larger than the characteristic field of the dipole-dipole interaction $B_{dd} = 1.5$ G? We suggest that this is made possible by the multi-isotope nature of the NSS in GaAs. Since quadrupole splittings and gyromagnetic ratios of the three isotopes are all different, the NSS of GaAs can demonstrate a rich variety of possible inter-isotope flip-flop transitions. These transitions frequencies ν_N are illustrated in Fig. 4 as functions of the magnetic field

in the absence (Fig. 4(a)) and in the presence of the quadrupole splitting of the nuclear spin states along z -axis (Fig. 4 (c, e)). The spin flip-flop transitions involving different isotopes ensure the energy transfer between the Zeeman and quadrupole energy reservoirs, with total energy conservation of the NSS. These transitions are broadened by dipole-dipole interactions. It is usually assumed⁴ that the efficient equilibration of energy reservoirs is ensured at detuning from the resonance less than $\delta\nu_N = 5B_{dd}/(2\pi\langle\gamma_N\rangle) = 8$ kHz (yellow band). One can see in Fig. 3(d,f), that for both orientations of the magnetic field, the transitions involving such a small detuning are available at $B < 50$ G, and the mixing remains as efficient as in the absence of the quadrupole splitting (Fig. 3(b)).

Our results show that the strain-induced nuclear quadrupole splittings in semiconductor microcavity do not hinder the establishment of the thermodynamic equilibrium within the nuclear spin system. The quadrupole effects result in the increase of the local field, indicating that the heat capacity of the NSS is dominated by the quadrupole energy reservoir. The energy transfer between the Zeeman and quadrupole reservoirs during

adiabatic demagnetisation is made possible by dipole-dipole interaction via spin flip-flop transitions involving different isotopes. Thus, deep cooling of the NSS down to microKelvin temperature range via adiabatic demagnetisation is possible in photonic microstructures. This paves the way towards realization of nuclear magnetically ordered states and their applications, including spin-photon interfaces with reduced noise.

ACKNOWLEDGMENTS

This work was supported by the joint grant of the Russian Foundation for Basic Research (RFBR, Grant No. 16-52-150008) and National Center for Scientific Research (CNRS, PRC SPINCOOL No. 148362), as well as French National Research Agency (Grant OBELIX, No. ANR-15-CE30-0020-02). IIR, VSZ and GGK acknowledge Russian Science Foundation (grant No. 17-12-01124) for the financial support of their experimental work.

-
- ¹ G. R. Pickett, Rep. Prog. Phys. **51**, 1295 (1988).
 - ² T. A. Knuuttila, J. T. Tuoriniemi, K. Lefmann, K. I. Jun-tunen, F. B. Rasmussen, and K. K. Nummilla, J Low Temp Phys **123**, 65 (2001).
 - ³ P. J. Hakonen, S. Yin, and O. V. Lounasmaa, Phys. Rev. Lett. **64**, 2707 (1990).
 - ⁴ A. S. Oja and O. V. Lounasmaa, Rev. Mod. Phys. **69**, 1 (1997).
 - ⁵ N. Kurti, F. N. H. Robinson, F. Simon, and D. A. Spohr, Nature **178**, 450 (1956).
 - ⁶ F. Pobell, *Matter and Methods at Low Temperatures*, 3rd ed. (Springer-Verlag, 2007).
 - ⁷ J. Tuoriniemi, Nat Phys **12**, 11 (2016).
 - ⁸ A. Abragam and W. G. Proctor, Physical Review **109**, 1441 (1958).
 - ⁹ A. Abragam and W. G. Proctor, physical review **106**, 160 (1957).
 - ¹⁰ M. Chapellier, M. Goldman, V. H. Chau, and A. Abragam, J. Appl. Phys. **41**, 849 (1970).
 - ¹¹ M. Goldman, M. Chapellier, V. H. Chau, and A. Abragam, Phys. Rev. B **10**, 226 (1974).
 - ¹² A. L. Falk, P. V. Klimov, V. Ivády, K. Szász, D. J. Christle, W. F. Koehl, Á. Gali, and D. D. Awschalom, Phys. Rev. Lett. **114**, 247603 (2015).
 - ¹³ E. A. Chekhovich, A. Ulhaq, E. Zallo, F. Ding, O. G. Schmidt, and M. S. Skolnick, Nature Materials **16**, 4959 (2017).
 - ¹⁴ M. Goldman, *Spin temperature and nuclear magnetic resonance in solids*, International series of monographs on physics (Clarendon Press, 1970).
 - ¹⁵ W. K. Rhim, A. Pines, and J. S. Waugh, Phys. Rev. Lett. **25**, 218 (1970).
 - ¹⁶ W. K. Rhim, A. Pines, and J. S. Waugh, Phys. Rev. B **3**, 684 (1971).
 - ¹⁷ V. Kalevich, V. Kulkov, and V. Fleisher, Izvestiya Akademii Nauk SSSR Seriya Fizicheskaya **46**, 492 (1982).
 - ¹⁸ P. Maletinsky, M. Kroner, and A. Imamoglu, Nat Phys **5**, 407 (2009).
 - ¹⁹ A. Kavokin, J. J. Baumberg, G. Malpuech, and F. P. Laussy, *Microcavities*, Series on Semiconductor Science and Technology (OUP Oxford, 2007).
 - ²⁰ I. A. Merkulov, Soviet Physics JETP **55**, 188 (1982).
 - ²¹ I. Merkulov, Physics of the Solid State **40**, 930 (1998).
 - ²² D. Scalbert, Phys. Rev. B **95**, 245209 (2017), arXiv:1703.05987.
 - ²³ C. Arnold, J. Demory, V. Loo, A. Lemaître, I. Sagnes, M. Glazov, O. Krebs, P. Voisin, P. Senellart, and L. Lanco, Nature Communications **6**, 6236 (2015).
 - ²⁴ R. Stockill, C. Le Gall, C. Matthiesen, L. Huthmacher, E. Clarke, M. Hugues, and M. Atatüre, Nature Communications **7**, 12745 (2016).
 - ²⁵ S. Sun, H. Kim, G. S. Solomon, and E. Waks, Nature Nanotech **11**, 539 (2016).
 - ²⁶ W. B. Gao, P. Fallahi, E. Togan, J. Miguel-Sanchez, and A. Imamoglu, Nature **491**, 426 (2012).
 - ²⁷ M. I. Dyakonov and V. I. Perel, Soviet Physics JETP **38**, 177 (1974).
 - ²⁸ V. K. Kalevich, K. V. Kavokin, I. Merkulov, and M. R. Vladimirova, “Dynamic nuclear polarization and nuclear fields,” in *Spin Physics in Semiconductors*, edited by M. I. Dyakonov (Springer International Publishing, Cham, 2017) pp. 387–430.
 - ²⁹ For the sake of simplicity we completely neglect the spin-lattice relaxation, and the related lost of polarization due to this process.
 - ³⁰ F. Meier and B. Zakharchenya, eds., *Optical orientation*, Modern Problems in Condensed Matter Science Series, Vol. 8 (North-Holland, Amsterdam, 1984).

- ³¹ E. Artemova and I. Merkulov, *Sov. Phys. Solid State* **27**, 941 (1985).
- ³² R. Giri, S. Cronenberger, M. Vladimirova, D. Scalbert, K. V. Kavokin, M. M. Glazov, M. Nawrocki, A. A. Lemaître, and J. Bloch, *Phys. Rev. B* **85**, 195313 (2012).
- ³³ R. Giri, S. Cronenberger, M. M. Glazov, K. V. Kavokin, A. Lemaître, J. Bloch, M. Vladimirova, and D. Scalbert, *Phys. Rev. Lett.* **111**, 087603 (2013).
- ³⁴ I. I. Ryzhov, S. V. Poltavtsev, K. V. Kavokin, M. M. Glazov, G. G. Kozlov, M. Vladimirova, D. Scalbert, S. Cronenberger, A. V. Kavokin, A. Lemaître, J. Bloch, and V. S. Zapasskii, *Appl. Phys. Lett.* **106**, 242405 (2015).
- ³⁵ F. Berski, J. Hübner, M. Oestreich, A. Ludwig, A. D. Wieck, and M. Glazov, *Phys. Rev. Lett.* **115**, 176601 (2015).
- ³⁶ S. Cronenberger, D. Scalbert, D. Ferrand, H. Boukari, and J. Cibert, *Nature Communications* **6**, 8121 (2015).
- ³⁷ I. I. Ryzhov, G. G. Kozlov, D. S. Smirnov, M. M. Glazov, Y. P. Efimov, S. A. Eliseev, V. A. Lovtcius, V. V. Petrov, K. V. Kavokin, A. V. Kavokin, and V. S. Zapasskii, *Sci. Rep.* **6**, 21062 (2016).
- ³⁸ Starting the field scan at $B_z^i = 50$ G, rather than at $B_z^p = 180$ G is chosen to limit the duration of the scan, and thus nuclear spin relaxation.
- ³⁹ M. Vladimirova, S. Cronenberger, D. Scalbert, M. Kotur, R. I. Dzhirov, I. I. Ryzhov, G. G. Kozlov, V. S. Zapasskii, A. Lemaître, and K. V. Kavokin, *Phys. Rev. B* **95**, 125312 (2017).
- ⁴⁰ D. Paget, G. Lampel, B. Sapoval, and V. Safarov, *Physical Review B* **15**, 5780 (1977).
- ⁴¹ Same measurements were done in Sample B, see SM.
- ⁴² We have checked that this value is not affected neither by pumping duration and power (that change Θ_{N0}), nor by increasing probe power (that eventually broadens the SN peak). Note also that the low frequency signal that appears in the bulk sample results from the spatial regions where nuclei are not polarized by the pump.
- ⁴³ M. Kotur, R. I. Dzhirov, M. Vladimirova, B. Jouault, V. L. Korenev, and K. V. Kavokin, *Phys. Rev. B* **94**, 081201 (2016).
- ⁴⁴ Details are given in Supplemental Material. Strong low-frequency signal in Fig. 3(c,d) is due to electrons that do not experience the influence of nuclei.
- ⁴⁵ K. Flisinski, I. Y. Gerlovin, I. V. Ignatiev, M. Y. Petrov, S. Y. Verbin, D. R. Yakovlev, D. Reuter, A. D. Wieck, and M. Bayer, *Phys. Rev. B* **82**, 081308 (2010).
- ⁴⁶ M. Eickhoff, B. Lenzmann, D. Suter, S. E. Hayes, and A. D. Wieck, *Phys. Rev. B* **67**, 085308 (2003).